

1 **Imaging flow cytometry challenges the usefulness of classically used EV**  
2 **labelling dyes and qualifies that of a novel dye, named Exoria™ for the**  
3 **labelling of MSC-EV preparations**

4 Exoria, a novel lipid dye for the EV-labelling

5 Tobias Tertel<sup>1</sup>, Melanie Schoppet<sup>2</sup>, Oumaima Stambouli<sup>1</sup>, Ali Al-Jipouri<sup>1</sup>, Patrick F. James<sup>2</sup>,  
6 Bernd Giebel<sup>1</sup>

7 <sup>1</sup>Institute for Transfusion Medicine, University Hospital Essen, University of Duisburg-Essen,  
8 Essen, Germany

9 <sup>2</sup>Exopharm Ltd, Level 17, 31 Queen St, Melbourne, Victoria, Australia

10 **Correspondence:**

11 Bernd Giebel, Ph.D.,  
12 Institute for Transfusion Medicine,  
13 University Hospital Essen,  
14 Virchowstr. 179, 45147 Essen, Germany  
15 Tel.: +49-201-7234204; FAX: +49-201-7235906  
16 E-mail: bernd.giebel@uk-essen.de

17 **Abstract**

18 Extracellular vesicles (EVs) are involved in mediating intercellular communication processes.  
19 An important goal within the EV field is the study of the biodistribution of EVs and the  
20 identification of their target cells. Considering that EV uptake is central for mediating the EVs  
21 role in intercellular communication processes, labelling with fluorescent dyes has emerged  
22 as a broadly distributed strategy for the identification of the EVs target cells and tissues.  
23 However, the accuracy and specificity of commonly utilized labelling dyes has not been  
24 sufficiently analyzed. By combining recent advancements in imaging flow cytometry for the

25 phenotypic analysis of single EVs and aiming to identify target cells for EVs within  
26 therapeutically relevant MSC-EV preparations, we explored the EV labelling efficacy of  
27 various fluorescent dyes, specifically of CFDA-SE, Calcein AM, PKH67, BODIPY-TR-  
28 Ceramide and a novel lipid dye named Exoria. Our analyses qualified Exoria as the only dye  
29 which specifically labels EVs within our MSC-EV preparations. Furthermore, we demonstrate  
30 Exoria labelling does not interfere with the immunomodulatory properties of the MSC-EV  
31 preparations as tested in a multi-donor mixed lymphocyte reaction assay. Within this assay,  
32 labelled EVs were differentially taken-up by different immune cell types. Overall, our results  
33 qualify Exoria as an appropriate dye for the labelling of EVs derived from our MSC-EV  
34 preparations, this study also demonstrates the need for the development of next generation  
35 EV characterization tools which are able to localize and confirm specificity of EV labelling.

36 **Keywords:** extracellular vesicles, EVs, exosomes, microvesicles, microparticles, vesicles,  
37 imaging flow cytometry, IFCM, analyses of EVs, lipid dye

## 38 **Introduction**

39 Extracellular vesicles (EVs) are membrane-enclosed particles in the nano- and micrometer  
40 range that are secreted into their extracellular environment by virtually all cells. According to  
41 their origin EVs are classified into different groups. The most prominent groups are  
42 exosomes, derivatives of the endosomal system with size ranges of 70-150 nm,  
43 microvesicles, shed off of the plasma membrane of 100-1,000 nm, and apoptotic vesicles  
44 that can be as small as exosomes and as apoptotic bodies can reach sizes up to several  
45 micrometers (Raposo and Stoorvogel, 2013).

46 Despite these classes, EVs of each given subtype are very heterogeneous as well.  
47 Depending on the cell source they are originating from, they provide specific molecular  
48 compositions, qualifying them as a new class of biomarkers. Specifically, EVs residing in the  
49 plasma are increasingly used as biomarkers for different diseases (Fais et al., 2016; König et  
50 al., 2018; Vacchi et al., 2020). In addition to conventional methods, such as cytokine assays

51 or cellular analyses, the prevalence of selected EV subpopulations can provide important  
52 new information on the course of respective diseases.

53 It became evident that EVs are of physiological relevance and mediate complex intercellular  
54 interactions at local and remote sites, both under healthy and pathological conditions (Yanez-  
55 Mo et al., 2015). Thus, it is a goal of many EV researchers to dissect such intercellular  
56 communication processes in a magnitude of different biological processes. In this context it is  
57 a relevant task to identify EV target cells. Addressing this challenge, it evolved as a common  
58 strategy to use fluorescent dyes considered to specifically label EVs and to apply labelled EV  
59 fractions either to assumed target cells/tissues *in vitro* or apply them *in vivo*. Among the  
60 commonly used dyes are dyes immediately integrating into membranes such as PKH dyes,  
61 dyes which become fluorescent after enzymatic reactions like non-fluorescent  
62 carboxyfluorescein diacetate succinimidyl ester (CFDA-SE) which by esterase is processed  
63 into carboxyfluorescein succinimidyl ester (CFSE), Calcein acetoxymethyl (Calcein AM)  
64 which binds calcium cations to become fluorescent or 4,4-difluoro-4-bora-3a,4a-diaza-s-  
65 indacene (BODIPY) conjugated fatty acids, e.g. ceramide (Chuo et al., 2018; Gray et al.,  
66 2015; Laulagnier et al., 2005; Nazarenko et al., 2013; Pospichalova et al., 2015; Pužar  
67 Dominkuš et al., 2018). Due to their micelle forming capabilities, use of several of these dyes  
68 are challenging for the EV field. Sophisticated preparation and washing procedures need to  
69 be followed to efficiently deplete dye aggregates, very often resulting in minor recovery rates  
70 (Dehghani et al., 2020). Furthermore, some dyes such as CFDA-SE require specific  
71 enzymatic activities to become fluorescent, in this case an esterase, to bind EV associated  
72 proteins and thus to efficiently label EVs (Banks et al., 2013).

73 For the quality control of dye labelled EV fractions, particle quantification methods are  
74 commonly used, and often performed by nanoparticle tracking analysis (NTA) or resistive  
75 pulse sensing. In 2011, our group in addition to Dragovic and co-workers introduced NTA as  
76 an “exosome” quantification method (Dragovic et al., 2011; Sokolova et al., 2011). However,  
77 the detailed comparison of data recorded using NTA and imaging flow cytometry (IFCM) (a  
78 more advanced EV characterization method), indicated that particle quantification methods

79 are not appropriate to calculate EV concentrations in EV samples - unless they are ultra-pure  
80 (Droste et al., 2021). This cannot be achieved with conventional EV preparation techniques  
81 such as differential centrifugation, polymer precipitation or simple size exclusion technologies  
82 (Droste et al., 2021; Karimi et al., 2018; Vergauwen et al., 2017). In their traditional form,  
83 particle quantification methods cannot distinguish prepared particles such as protein  
84 precipitates, salt crystals and lipoprotein agglomerates from EVs. In addition, light scattering  
85 based methods can only detect some of the particles smaller than 100 nm due to their limited  
86 sensitivity (Giebel and Helmbrecht, 2017; van der Pol et al., 2014). Provided EVs are  
87 fluorescently labelled, IFCM grants an advanced platform for single EV detection (Görgens et  
88 al., 2019). Recently, we have optimized antibody labelling protocols for single EV analysis  
89 (Görgens et al., 2019; Tertel et al., 2020a; Tertel et al., 2020b). These protocols allowed us  
90 to investigate whether tetraspanins, specifically CD9, CD63 and CD81, whose expression  
91 within EV samples has been confirmed by WB, are co-localized on individual EVs or are  
92 recovered on distinct EV subsets. With this technology we analyzed EV preparations from  
93 mesenchymal stromal cell (MSC) conditioned, human platelet lysate supplemented media,  
94 whose therapeutic activities we study in different animal models and confirmed their  
95 therapeutic potential in a GvHD patient (Doepfner et al., 2015; Drommelschmidt et al., 2017;  
96 Kaminski et al., 2020; Kordelas et al., 2014; Ophelders et al., 2016; Wang et al., 2020). We  
97 demonstrated that CD9 and CD81 reside on different EV subpopulations all in the exosomal  
98 size range (Görgens et al., 2019). Notably, these results had been confirmed by an  
99 advanced multiplex bead-capturing procedure (Wiklander et al., 2018). Considering the  
100 method of IFCM as very informative for the EV characterization and intending to qualify a  
101 pan-EV labelling dye, we thus decided to evaluate the EV labelling efficacy of different dyes  
102 being used for EV marking. In addition to conventionally used BODIPY-TR-CER, Calcein  
103 AM, CFSE and PKH67 dyes, we included a novel dye named Exoria in our studies. Exoria,  
104 developed at Exopharm Ltd, was designed to be a pH stable fluorescence dye with reduced  
105 micelle forming propensity, which could incorporate into EVs.

106 In this study, the labelling efficiency of MSC-EV preparations with the dyes listed above was  
107 investigated. Counterstaining of PKH67 and Exoria labelled objects was performed with anti-  
108 tetraspanin antibodies. The impacts of Exoria labelling on the immunomodulatory capabilities  
109 of the MSC-EV preparation were investigated in a multi-donor mixed lymphocyte reaction  
110 (mdMLR) assay. Furthermore, the uptake of Exoria labelled objects by the different immune  
111 cells within the mdMLR assay were documented.

## 112 **Material and methods**

### 113 **Preparation of EVs from MSC conditioned cell culture media**

114 MSC-EVs were prepared from human platelet lysate containing MSC-conditioned media by  
115 polyethylene glycol 6000 precipitation followed by ultracentrifugation, as described previously  
116 (Borger et al., 2020; Kordelas et al., 2014; Ludwig et al., 2018). Conditioned media were  
117 harvested every 48 h. Obtained MSC-EV preparations were diluted in NaCl-HEPES buffer  
118 (Sigma-Aldrich, Taufkirchen, Germany) such that 1 mL of final samples contained the  
119 preparation yield of the conditioned media of approximately  $4.0 \times 10^7$  cells.

### 120 **Characterization of the EV preparations**

121 Obtained EV preparations were characterized according to the MISEV criteria (They et al.,  
122 2018). Briefly, average particle concentrations were determined by NTA on a ZetaView PMX-  
123 120 platform equipped with the software version 8.03.08.02 (ParticleMetrix, Meerbusch,  
124 Germany) as described previously (Ludwig et al., 2018). Protein concentration was  
125 determined by bicinchoninic acid (BCA) assay (Pierce, Rockford, IL, USA) in 96-well plates  
126 according to the manufacturer's recommendations. The presence of EV specific proteins  
127 (CD9, CD63, CD81 and Syntenin) and the absence of impurities (Calnexin) were confirmed  
128 in Western Blots performed as described previously (Ludwig et al., 2018).

### 129 **EV labelling with different dyes**

130 The staining with CFSE (Thermo Fisher Scientific, Darmstadt, Germany) was based on the  
131 manufacturer's protocol. Slight modifications were required to reduce the signal from

132 unbound CFSE. Briefly, the CFSE stock solution was diluted to a working solution of 10  $\mu$ M  
133 CFSE. The solution was centrifuged three times for 10 min at 17,000  $\times g$  (see also  
134 supplement figure 1). Subsequently, 25  $\mu$ L of MSC-EV preparations, corresponding to the  
135 amount of EVs derived from  $1 \times 10^6$  MSCs, were incubated with the centrifuged CFSE solution  
136 for 20 min at 37°C. The sample was diluted 1:20 to a final volume of 1 mL prior to analysis.

137 The staining of MSC-EV preparations with Calcein AM followed the manufacturer's  
138 instructions. Briefly, 25  $\mu$ L of MSC-EV preparations were incubated with 25  $\mu$ L of a 20  $\mu$ M  
139 solution of Calcein AM (Thermo Fisher Scientific) for 40 min at 37°C. The sample was diluted  
140 1:20 to a final volume of 1 mL to reduce background noise, avoiding the requirement of a  
141 washing step.

142 The staining of MSC-EV preparations with BODIPY-TR-Ceramide followed the  
143 manufacturer's instructions. Briefly, 25  $\mu$ L of the MSC-EV preparation, corresponding to EVs  
144 purified from  $4 \times 10^6$  MSCs, were incubated with 25  $\mu$ L of a 20  $\mu$ M solution of BODIPY TR  
145 Ceramide (Thermo Fisher Scientific) for 20 min at 37°C. 450  $\mu$ L of 0.9% NaCl with 10mM  
146 HEPES (0.9% NaCl, Melsungen, B. Braun; HEPES, Thermo Fisher Scientific) buffer was  
147 added and the EVs were washed by using a Centrifugal Concentrator (Vivaspin 500;  
148 Sartorius, Göttingen, Germany). The retentate was adjusted to 500  $\mu$ L prior to analysis.

149 The staining of MSC-EV preparations with PKH67 followed the manufacturer's instructions  
150 for labeling EVs (Thermo Fisher Scientific). Briefly, using 200  $\mu$ L of given MSC-EV  
151 preparations, corresponding to EVs purified from  $8 \times 10^6$  cells, the solution was adjusted with  
152 Diluent C to a final volume of 1 mL. 6  $\mu$ L of PKH67 dye was added to each tube and mixed  
153 continuously for 30 seconds. After 5 min at room temperature, the solution was quenched by  
154 adding 2 mL of 10% (w/v) bovine serum albumin fraction 5 (Carl Roth, Karlsruhe, Germany).  
155 Serum-free medium, DMEM low glucose (PAN Biotech, Aidenbach, Germany) supplemented  
156 with 100 U/ mL penicillin-streptomycin-glutamine (Thermo Fisher Scientific, Darmstadt,  
157 Germany), was used to adjust the volume to 8.5 mL. 1.5 mL of a 0.971 M sucrose solution  
158 (Carl Roth) was added to the bottom of the tube, and the tube was centrifuged for 2 hours at

159 190,000 x g in a swing-out rotor (SW40 Ti; Beckman Coulter, Krefeld, Germany; k-factor:  
160 137) at 4 °C. The supernatant was discarded, and the pellet resuspended in Na-HEPES  
161 buffer. After resuspension, the volume was adjusted to 5 mL and transferred to a Centrifugal  
162 Concentrator (Vivaspin 6; Sartorius). The retentate was adjusted to 120 µL prior to analysis.

163 The MSC-EV preparations were stained with Exoria following the protocol provided by  
164 Exopharm Ltd. Exoria was provided as a lyophilized powder. 1 mg was resuspended with 1  
165 mL buffer to a final concentration of 0.2 µM. Like CFDA-SE, the Exoria solution was  
166 centrifuged for 10 min at 17,000 x g to reduce background noise to a minimum. Briefly, for  
167 the EV-labelling 25 µL of the MSC-EV preparations were incubated with 25 µL of a prepared,  
168 centrifuged Exoria solution (0.2 µM) for 1 hour at 37°C. The sample was diluted 1:20 to a  
169 final volume of 1 mL prior to analysis. For EV uptake experiments Exoria labelled MSC-EV  
170 preparations were cleared from EV unbound Exoria by ultrafiltration. Briefly, after labelling  
171 with Exoria, the MSC-EVs were washed by via centrifugation at 12,000xg through Vivaspin  
172 500 filters (Sartorius) for 10 min. The retentate was collected as labelled EV sample.

### 173 **Antibody labelling of prepared EVs**

174 After dye labelling, 5 µL of Exoria stained MSC-EV samples were mixed with 20 µL of a 10  
175 nM anti-human CD9 FITC (EXBIO, Vestec, Czech Republic), 12 nM anti-human CD63  
176 AF488 (EXBIO) or 13 nM anti-human CD81 FITC (Beckman Coulter) antibody solution,  
177 respectively. For PKH67 stained MSC-EV samples, incubated with 10 nM anti-human CD9  
178 PE (EXBIO), 12 nM anti-human CD63 PE (EXBIO) or 13 nM anti-human CD81 PE (Beckman  
179 Coulter), respectively, for 2 hours at room temperature as described previously (Tertel et al.,  
180 2020b). Accordingly, isotype controls were performed (see also supplement table 1) For  
181 Exoria, final preparations were diluted to 500 µL for CD9 (end dilution factor of 1 to 100) and  
182 200 µL for CD63 and CD81 analyses (end dilution factor of 1 to 40). The preparations for  
183 PKH67 were diluted to 100 µL for all three analyses (1:20 dilution).

### 184 **Detergent control**

185 To test for the EV nature of labelled objects detergent controls were performed by adding a  
186 sample volume of a 2% (w/v) NP-40 solution (Calbiochem, San Diego, CA, USA) to the  
187 samples.

### 188 **IFCM analyses**

189 All samples were measured using the built-in autosampler from U-bottom 96-well plates  
190 (Corning Falcon, cat 353077) with 5 min acquisition time per well on the AMNIS  
191 ImageStreamX Mark II Flow Cytometer (AMNIS/Luminex, Seattle, WA, USA). All data were  
192 acquired at 60x magnification at low flow rate ( $0.3795 \pm 0.0003 \mu\text{L}/\text{min}$ ) and with removed  
193 beads option deactivated as described previously (Görgens et al., 2019; Tertel et al., 2020a).  
194 The data was analyzed as described previously (Tertel et al., 2020b). Additional settings can  
195 be found in supplement table 2 and 3.

### 196 **Multi-donor mixed lymphocyte reaction (mdMLR)**

197 The immunomodulatory potential of Exoria labelled and non-labelled MSC-EV preparations  
198 were compared in a multi-donor mixed lymphocyte reaction assay (MLR) exactly as  
199 described previously (Madel et al., 2020). Briefly, Ficoll prepared peripheral blood  
200 mononuclear cells (PBMC) of 12 healthy donors were mixed in equal proportions, aliquoted  
201 and stored in the vapour phase of liquid nitrogen until usage. After thawing 600,000 cells  
202 were seeded per well of a 96-well U-bottom shape plates (Corning, Kaiserslautern,  
203 Germany) and cultured in 10% human AB serum (produced in house) and 100 U/mL  
204 penicillin and 100  $\mu\text{g}/\text{mL}$  streptomycin (Thermo Fisher Scientific) supplemented RPMI 1640  
205 medium (Thermo Fisher Scientific) in a final volume of 200  $\mu\text{L}$  per well, either in the presence  
206 or absence of MSC-EV preparations to be tested. After 5 days, cells were harvested, stained  
207 with a collection of different fluorescent labelled antibodies (CD4-BV785; BioLegend, San  
208 Diego, CA, USA; CD25-PE-Cy5.5; BD Bioscience; and CD54-AF700; EXBIO) and analysed  
209 on a Cytotflex flow cytometer (Software CytExpert 2.3, Beckman-Coulter). Activated and non-  
210 activated CD4<sup>+</sup> T cells were discriminated by means of their CD25 and CD54 expression,  
211 respectively. Typically, 5  $\mu\text{L}$  of MSC-EV preparations to be tested were applied into



212 respective wells. The following antibodies were used to further discriminate subpopulations:  
213 CD8-BV650 (BioLegend), CD14-PO (EXBIO), CD19-ECD (Beckman Coulter) and CD56-  
214 APC (BioLegend). The evaluation of the data was carried out with the Kaluza software  
215 (Version 2.1, Beckman Coulter).

## 216 **Statistics**

217 The statistics and graphical presentation were performed with GraphPad version 8.4.3. Mean  
218 values  $\pm$  standard deviation are provided.

## 219 **Results**

### 220 **CFSE, Calcein AM and BODIPY-TR-Ceramide do not label MSC-EVs**

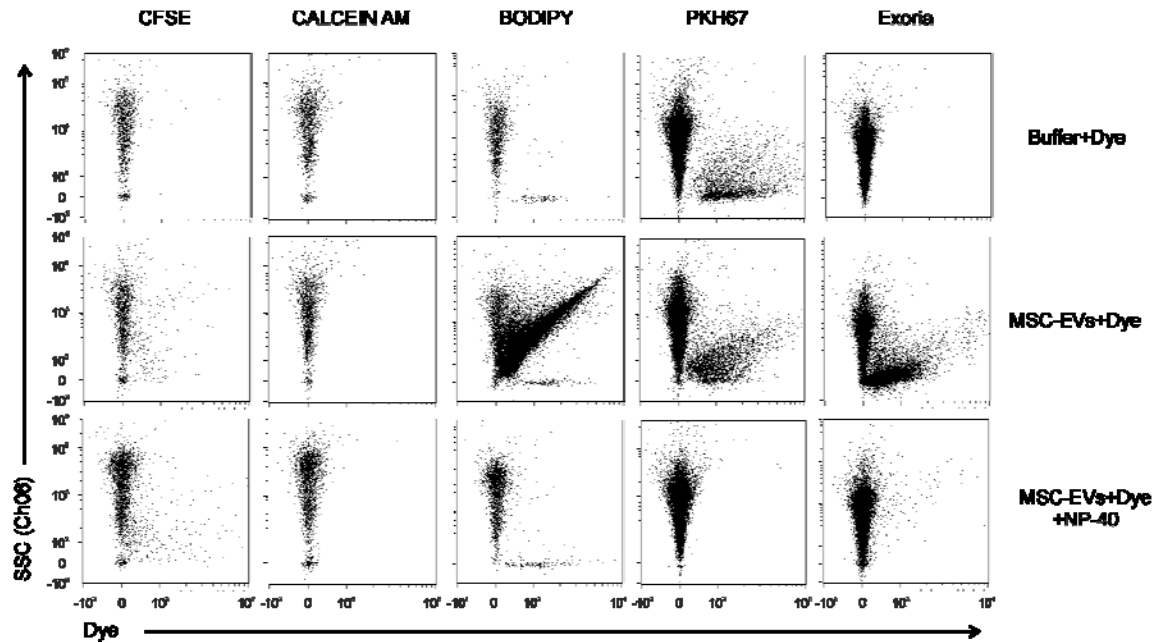
221 Aiming to identify a dye allowing specific labelling of EVs in therapeutically active MSC-EV  
222 preparations, we decided to evaluate the accuracy of conventionally used EV labelling dyes,  
223 specifically CFSE, Calcein AM, PKH67, BODIPY-TR-Ceramide and a novel lipid dye named  
224 Exoria. MSC-EV preparations that have been extensively explored in various animal models  
225 had been obtained from supernatants of MSCs raised in 10% human platelet lysate  
226 supplemented media by our well established PEG-ultracentrifugation protocol (Borger et al.,  
227 2020; Doeppner et al., 2015; Drommelschmidt et al., 2017; Gussenhoven et al., 2019;  
228 Kaminski et al., 2020; Kordelas et al., 2014; Ludwig et al., 2018; Ophelders et al., 2016;  
229 Wang et al., 2020). Since micelle formation of some of the dyes have been reported and  
230 following the MIFlowCyt-EV recommendation (Welsh et al., 2020), we initially added all of the  
231 labelling dyes but the EV sample to the NaCl-HEPES buffer, the buffer MSC-EVs are  
232 suspended in. Samples were processed according to the manufacturer's recommendation  
233 and analyzed by IFCM with protocols that we have successfully established for the  
234 characterization of antibody labelled MSC-EVs (Görgens et al., 2019; Tertel et al., 2020a;  
235 Tertel et al., 2020b).

236 Notably, depending on the manufacturer's protocol, different amounts of MSC-EV  
237 preparation was required. For the CFSE, Calcein-AM, BODIPY-TR Ceramide-(BODIPY) and  
238 Exoria labelling we started with volumes of 25  $\mu$ L of MSC-EV preparation, for PKH67 with

239 200  $\mu$ L. Initially, we analyzed all recorded objects. Based on our prior experience, sEVs  
240 appear as fluorescently labelled objects with minimal side scatter signals (SSC). Upon  
241 comparing the dye only solutions, CFSE, Calcein AM and Exoria were observed to contain  
242 no objects. In contrast, upon analyzing the BODIPY and PKH67 solutions, solid populations  
243 of labelled objects with minimal side scatter signals were identified (Figure 1). This data  
244 implies micelle or aggregate formation of BODIPY and PKH dyes.

245 Subsequently, MSC-EV preparations labelled using the same procedure were analyzed. In  
246 contrast to the buffer only solutions, solid populations of labelled objects were observed after  
247 BODIPY, PKH67 and Exoria labelling and some objects following CFSE labelling (Figure 1).  
248 Calcein AM failed to label any detectable objects. BODIPY<sup>+</sup> objects that were not recovered  
249 in the buffer-BODIPY solution control revealed side scatter signals that were much higher  
250 than those typically seen for small EVs (sEVs). In contrast, the light scattering properties of  
251 the objects specifically labelled with PKH67 or Exoria reflect those of sEVs. Notably, in good  
252 agreement with published reports that PKH dyes increased the size of labelled EVs  
253 (Dehghani et al., 2020; Morales-Kastresana et al., 2017a), the PKH67<sup>+</sup> objects specifically  
254 labelled in the MSC-EV preparation indicated higher side scatter signals than Exoria<sup>+</sup> objects  
255 (Figure 1).

256 To determine whether the specifically labelled objects are detergent-sensitive, the dye-  
257 labelled MSC-EV samples was treated with NP40. While the BODIPY<sup>+</sup> objects specifically  
258 detected in MSC-EV preparations, those with the higher light scattering properties, and all  
259 PKH67<sup>+</sup> and Exoria<sup>+</sup> objects disappeared following NP40 treatment. In contrast, the  
260 population of CFSE<sup>+</sup> objects and the BODIPY<sup>+</sup> objects with sEV light scattering properties  
261 were hardly affected by the NP40 treatment. To this end, we considered neither detergent  
262 resistant CFSE<sup>+</sup> nor the BODIPY<sup>+</sup> objects with low light scattering properties as small EVs.  
263 Coupled to the failure of Calcein AM to label any specific objects, we excluded CFSE,  
264 Calcein AM and BODIPY from all later analyses and focused on exploring the accuracy of  
265 PKH67 and Exoria as MSC-EV labelling dyes.



266

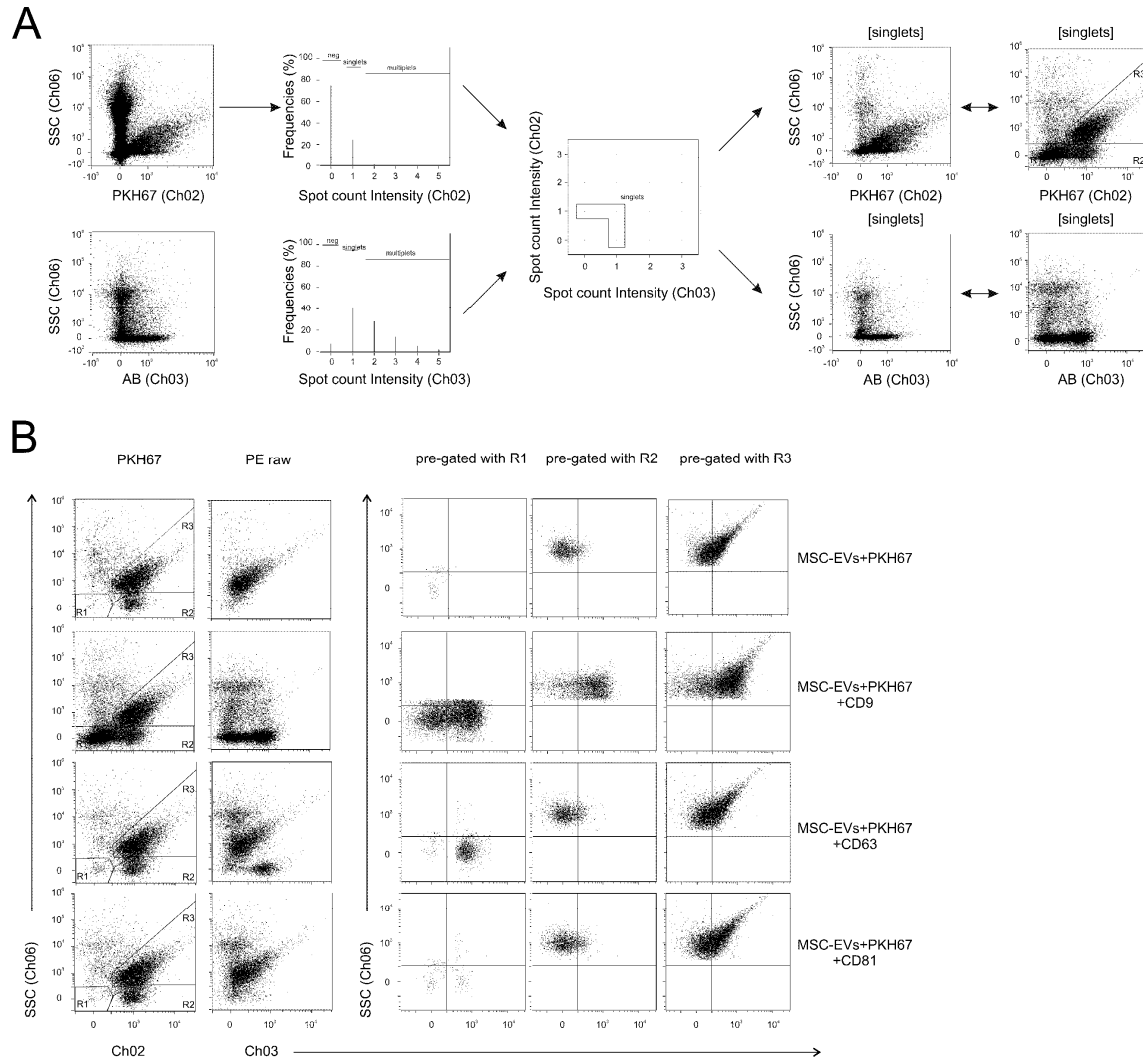
267 **Figure 1: PKH67 and Exoria specifically label objects within MSC-EV preparation with sEV-like**  
268 **side scatter properties.** Fluorescent labelling procedures were performed for CFSE, Calcein AM,  
269 BODIPY, PKH67 and Exoria in the absence of any EV preparation (upper row), and in the presence of  
270 MSC-EVs, alone (middle row) or in the presence of MSC-EVs and the detergent NP40. Fluorescence  
271 intensities of the dye labelled objects (x-axis) are plotted against the intensity of their size reflecting  
272 SSC signals (y-axis).

### 273 **PKH67 fails to effectively label CD9<sup>+</sup>, CD63<sup>+</sup> and CD81<sup>+</sup> sEVs**

274 Next, we investigated the potential co-localizations of PKH67 with known EV markers. To this  
275 end, we continued with the well characterized MSC-EV preparations. These were stained  
276 either by PKH67 alone or in combination with any of the following antibodies: anti-CD9, anti-  
277 CD81 or anti-CD63 antibodies. To reduce the background noise and to exclude coincident  
278 events, the simultaneous detection of two or more independent objects at the same time  
279 (coincidences with high object numbers), we applied an optimized gating strategy. Briefly, we  
280 focused on objects recognized as singlets in the PKH67 channel without a simultaneous  
281 antibody signal or as singlets in the antibody channel without a simultaneous PKH67 signal,  
282 and on events appearing in both channels as singlets not providing two individual objects  
283 (Figure 2A).

284 Upon plotting side scatter against PKH67 intensities, many more objects were recovered in  
285 samples that had been counterstained by anti-CD9 antibodies than in the PKH67 labelled  
286 buffer and MSC-EV containing controls. Most of these objects were negative for PKH67 and  
287 showed low SSC signals. The region containing these objects was defined as R1. For anti-  
288 CD9 staining,  $6672 \pm 1170$  objects were recovered in the region R1. Notably, hardly any  
289 objects were recovered in R1 in the PKH67 labelled MSC-EV samples that were not  
290 counterstained by antibodies. A slight increase in objects numbers was recorded when  
291 PKH67 labelled MSC-EV samples were counterstained with anti-CD63 ( $221 \pm 42$  objects) or  
292 anti-CD81 ( $96 \pm 32$  objects) antibodies. Most of the objects that were positive for PKH67  
293 revealed solid SSC signals. The region including these objects was defined as R3. A smaller  
294 number of PKH67 labelled objects was identified with low SSC signals that was clustered in  
295 a region defined as R2. In contrast to the number of objects in R1, the numbers of objects in  
296 R2 and R3 were only slightly affected by the antibody labelling procedures (Figure 2B and  
297 2C). Within the antibody non-labelled control  $2040 \pm 344$  objects were recovered in R2,  
298 following anti-CD9 staining  $2927 \pm 466$  objects, following anti-CD63 staining  $1747 \pm 141$   
299 objects and following anti-CD81 staining  $1734 \pm 200$  objects. In all antibody labelled MSC-EV  
300 preparations more objects were found in R3 (anti-CD9:  $6625 \pm 803$  objects; anti-CD63:  $5915$   
301  $\pm 271$  objects; anti-CD81:  $5777 \pm 675$  objects) than in the antibody non-labelled control ( $2046$   
302  $\pm 157$  objects). To analyze objects within the 3 different regions in more detail, their antibody-  
303 labelling intensities were plotted against PHK67 labelling intensities. The results clearly  
304 confirm that a huge proportion of the objects in R1 were effectively labelled by anti-CD9  
305 antibodies. Although the R1 object populations were much smaller following anti-CD63 and  
306 anti-CD81 than after anti-CD9 antibody staining, a proportion of these objects was clearly  
307 recognized as CD63<sup>+</sup> or CD81<sup>+</sup>, respectively (Figure 2B). In contrast, all objects in R2 or in  
308 R3 appeared as CD63<sup>-</sup> and CD81<sup>-</sup> objects, most of which can be labelled by anti-CD9  
309 antibodies. Notably, the frequencies of CD9<sup>+</sup>, CD63<sup>+</sup> and CD81<sup>+</sup> objects recovered in R1 are  
310 congruent to our previous observations that MSC-EV preparations contain a dominating  
311 CD9<sup>+</sup>CD81<sup>-</sup> and a minor CD9<sup>-</sup>CD81<sup>+</sup> sEV population (Görgens et al., 2019). Overall, we

312 consider that most antibody stained objects in R1 were sEVs not being labelled by PKH67  
 313 and that most of the sEVs can only be detected if they are successfully stained with any of the  
 314 3 antibodies. Thus, our data question PKH67 as efficient MSC-sEV labelling dye.



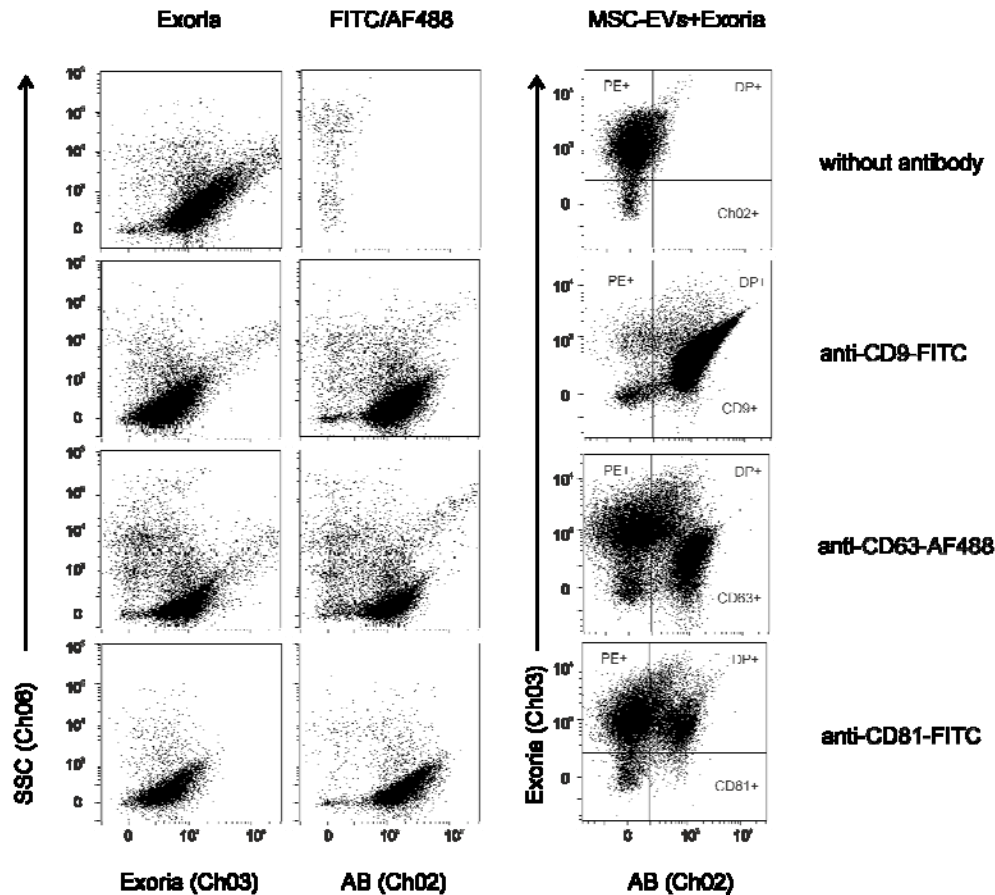
315

316 **Figure 2: PKH67 fails to effectively label small MSC-EVs.** (A) Gating strategy of the detected  
 317 objects. Exemplarily, the gating strategy is presented for MSC-EV preparations counterstained with  
 318 PKH67 and anti-CD9 antibodies. Both fluorescence channels (CH02 and CH03) are initially plotted  
 319 against the side scatter intensities (SSC) of all recorded objects. Number of co-incident objects per  
 320 channel are depicted (2<sup>nd</sup> column). Of all recorded objects, the only objects considered in subsequent  
 321 analyses were those that showed either single signals in the PKH67 or the antibody channel, or single  
 322 signals in both channels (singlets). Within the CH02 SSC singlet plots three different gates were  
 323 defined with singlets in R1 and R2 with low and in R3 with concrete side scatter signals. Objects in R1

324 revealed no PKH67 and those in R2 and R3 concrete PKH67 signals. Ch02 signals plotted against  
325 SSC signals of the singlets are shown as well, either in the same plot size as in the left column before  
326 gating or in the zoom in versions of the same plots (right column). (B) Distribution of recorded singlets  
327 in R1, R2 and R3 without antibody labelling or following anti-CD9, anti-CD63 or anti-CD81 labelling,  
328 respectively. Plotting of the fluorescence intensities of singlets in the PKH67 (Ch02) or the antibody  
329 channel (Ch03) against the singlets' side scatter intensities. Column 3 to 5, fluorescence intensities of  
330 R1 to R3 gated singlets. (C) Number of events in gates R1-R3 for the respective measurements. The  
331 mean values  $\pm$  standard deviation indicated.

### 332 **Exoria effectively labels CD9<sup>+</sup>, CD63<sup>+</sup> and CD81<sup>+</sup> EVs in MSC-EV preparations**

333 Next, the reliability of the Exoria as an EV labelling dye was investigated in a comparable  
334 manner to PKH67. To this end, the MSC-EV preparations (n=3) were either stained with  
335 Exoria alone or in combination with anti-CD9, anti-CD63 or anti-CD81 antibodies,  
336 respectively. Without defining R1-3 sub gates, gating strategies were applied as depicted in  
337 Figure 2A. In contrast to the PKH67 labelling experiments, many more objects with lower  
338 side scatter signal intensities were labelled by Exoria, even in the absence of any of the three  
339 different antibodies. No clear increase in the numbers of detected objects was observed  
340 between MSC-EV samples that were solely labelled by Exoria or in addition by anti-CD9  
341 antibodies (Figure 3). Thus, in contrast to the PKH67 labelling, Exoria labelling is sufficient to  
342 label most of the sEVs within our MSC-EV preparations. Interestingly, upon plotting the  
343 Exoria labelling intensities against that of the different antibodies, it appears that CD81<sup>+</sup>  
344 objects are more intensively labelled with Exoria than CD63<sup>+</sup> objects. Furthermore, the  
345 results imply that more than 90% of the CD9<sup>+</sup> and CD81<sup>+</sup> objects had been labelled with  
346 Exoria but only 60% of the CD63<sup>+</sup> EVs. All labelled objects were confirmed to be detergent  
347 sensitive (Suppl. Figure 2). Even though we do not have an explanation for the weaker  
348 Exoria stainability of CD63<sup>+</sup> compared to CD9<sup>+</sup> and CD81<sup>+</sup> objects, overall, the data  
349 demonstrate that Exoria successfully labels most of the sEVs in our MSC-EV preparations.



350

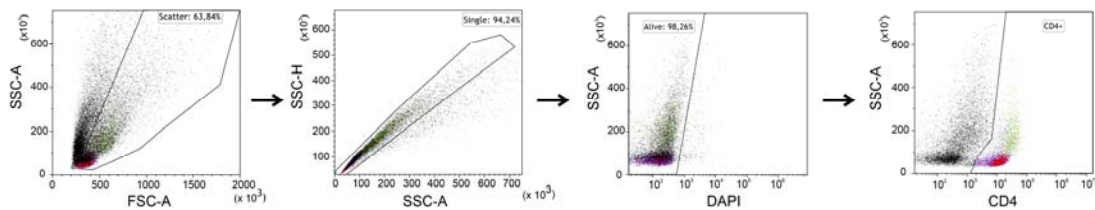
351 **Figure 3: Exoria stains tetraspanin containing EVs.** MSC-EV preparations were counterstained  
352 with Exoria and either anti-CD9, anti-CD63 or anti-CD81 antibodies. The same gating strategy as  
353 described in Figure 2 was applied. Fluorescence intensities of singlets are plotted against the side  
354 scatter (SSC) intensities either for the antibody (Ch02) or the Exoria (Ch03) channel. In the third  
355 column Exoria signals are plotted against the signals of respective antibodies. NP40 lysis controls are  
356 presented in Suppl. Figure 2.

### 357 **Exoria staining does not affect the immunomodulatory capacity of the MSC-EV** 358 **preparations**

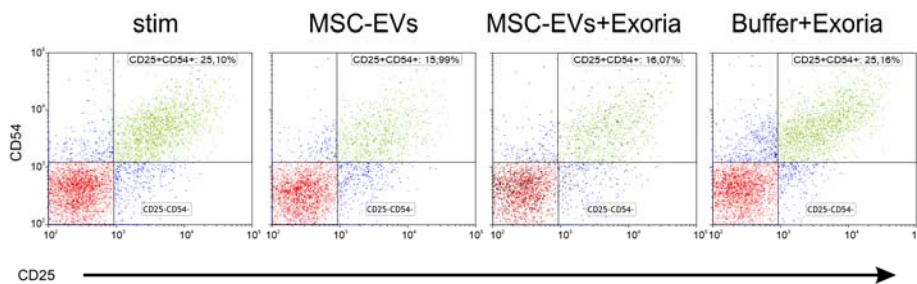
359 Next, we investigated whether Exoria affects the MSC-EV preparation's immunomodulatory  
360 capability. To this end, the activity of Exoria stained MSC-EV preparations were compared to  
361 corresponding, non-labelled MSC-EV preparations in a multi-donor mixed lymphocyte  
362 reaction (mdMLR) assay. Upon pooling of mononuclear cells from the peripheral blood of 12  
363 different healthy donors (PBMCs), allogenic immune reactions are induced that can be

364 monitored by the activation status of CD4<sup>+</sup> T cells. Following 5 days in culture, approximately  
365 a quarter of all CD4<sup>+</sup> T cells express the interleukin-2 receptor (CD25) and the intercellular  
366 adhesion molecule-1 (CD54), indicating T cell activation (Figure 4). As previously described,  
367 MSC-EV preparations with immunomodulatory capabilities effectively reduce the content of  
368 activated CD4<sup>+</sup> T cells (Madel et al., 2020). Consistently, in the presence of the non-labelled  
369 MSC-EV preparations only 16% of the monitored CD4<sup>+</sup> T cells were found to display the  
370 activation cell surface markers (Figure 4B). In the presence of Exoria labelled MSC-EV  
371 preparations (n=3) we observed a comparable reduction in CD4<sup>+</sup> T cell activation (Figure  
372 4B). Notably, Exoria itself did not influence the activation status of CD4<sup>+</sup> T cells (Figure 4B).  
373 Thus, Exoria does not recognizably affect the immunomodulatory capability of the applied  
374 MSC-EV preparations.

A



B



375

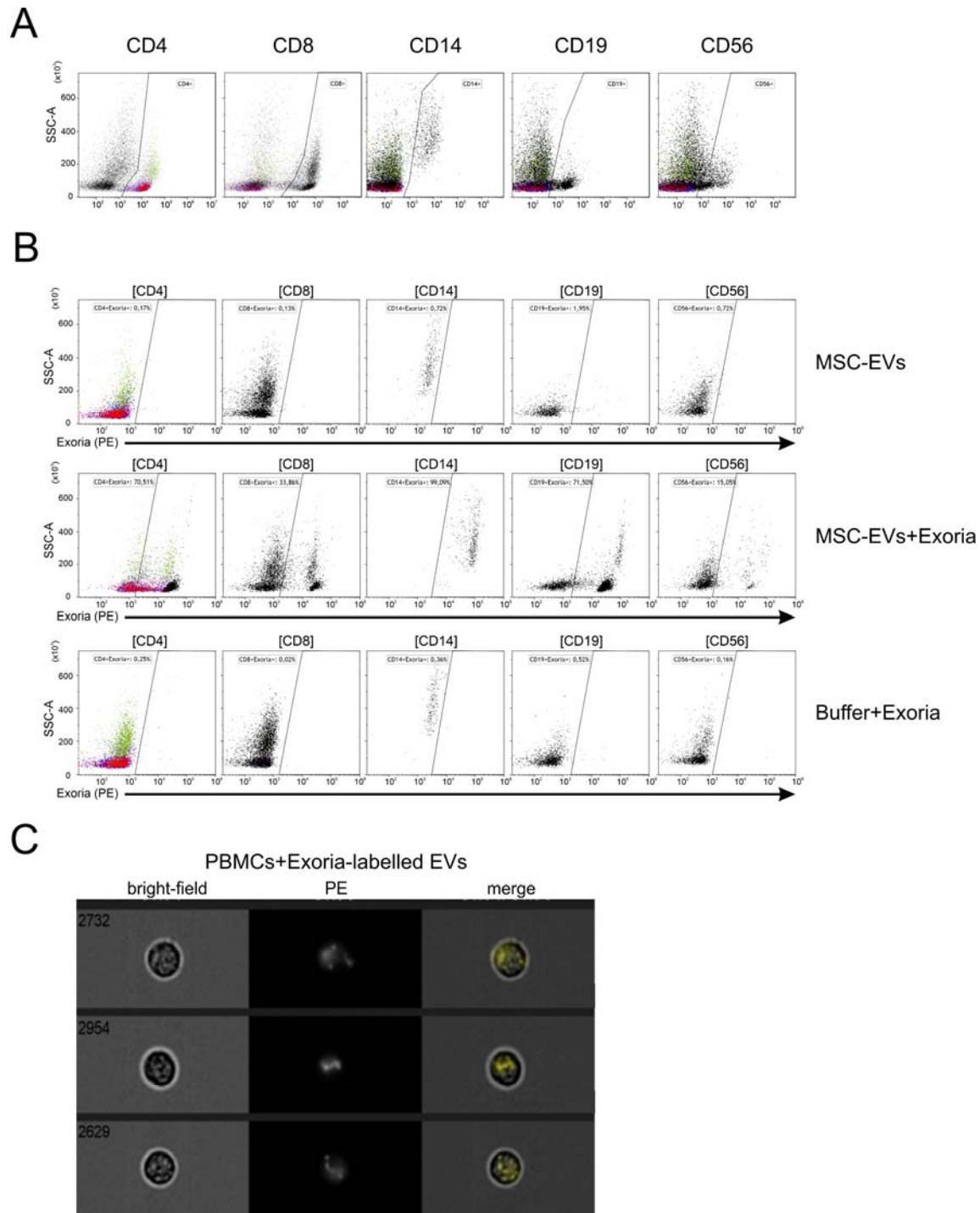
376 **Figure 4: Exoria staining does not affect the immunomodulatory capability of MSC-EV**  
377 **preparations.** Mixtures of PBMCs of 12 different donors were cultured in the presence or absence of  
378 non-labelled or Exoria labelled MSC-EV preparations, or in the presence of the Exoria dye for 5 days.  
379 Thereafter, cells were harvested and stained with DAPI and fluorescently labelled anti-CD4, anti-CD25  
380 and anti-CD54 antibodies and analyzed by conventional flow cytometry. (A) Gating strategy for CD4 T  
381 cells. Living cells were identified according to their forward and side scatter features as singlets and  
382 DAPI negative cells. CD4 T cells were gated as CD4<sup>+</sup> living cells. (B) Fluorescent intensities of CD25



383 *and CD54 gated living CD4<sup>+</sup> cells of mdMLR assays cultured in the absence of any additives (stim), in*  
384 *the presence of non-labelled MSC-EVs (MSC-EVs), Exoria labelled MSC-EVs (MSC-EVs +Exoria) or*  
385 *in the presence of buffer solved Exoria (Buffer + Exoria).*

386 **Exoria stain MSC-EVs exhibit different uptake potential across immune cell subtypes**  
387 **of a mdMLR assay**

388 To test whether Exoria EV labelling allows the identification of EV-up taking cells, we  
389 examined the labelled EV uptake of the different immune cells within the mdMLR assay,  
390 next. To this end, a pool of PBMCs derived from 12 healthy donors were cultured for 5 days  
391 in the presence of Exoria labelled MSC-EVs (n=3) that had been cleared from excessed  
392 Exoria dye by ultrafiltration. Thereafter, cells were harvested, antibody labelled and analyzed  
393 by flow cytometry. The content of Exoria labelled cells within different PBMC subtypes was  
394 determined. Almost all monocytes (CD14<sup>+</sup> cells, 99%) revealed Exoria signals. In contrast,  
395 only proportions of the different lymphocytes appeared as Exoria positive cells, i.e. 71% of all  
396 CD4<sup>+</sup> T cells (CD4<sup>+</sup> cells), 34% of all CD8<sup>+</sup> T cells (CD8<sup>+</sup> cells), 72% of all B cells (CD19<sup>+</sup>  
397 cells) and 15% of all NK cells (CD56<sup>+</sup> cells). In addition, IFCM was used to visualize the  
398 subcellular staining of Exoria positive cells (Figure 5C). Obtained images reveal concrete  
399 labelled structures that according to our experience are located subcellularly. Thus, Exoria  
400 labelled EVs within our MSC-EV preparations are specifically taken up by different contents  
401 of the immune cell types within the assay.



402

403 **Figure 5: Analyses of the various immune cell types within the mdMLR assay reveal**  
 404 **differences in uptake of Exoria-stained MSC-EVs.** Immune cells of the mdMLR were examined for  
 405 uptake of Exoria-stained MSC-EV preparations. (A) Discrimination of the different subpopulations was  
 406 performed by using antibodies against CD4 and CD8 (T cells), CD19 (B cells), CD56 (NK cells), and  
 407 CD14 (monocytes). (B) Different immune cells were examined for the presence of a signal for Exoria.

408 *Unstained MSC-EVs as well as a buffer control with Exoria were used as controls. (C) Analysis of the*  
409 *subcellular staining of following uptake of Exoria-stained EVs via imaging flow cytometry. Here, in*  
410 *addition to the light (bright field) and fluorescent microscopic images (PE channel; Exoria) merged*  
411 *images are shown.*

## 412 **Discussion**

413 Within this study we have evaluated the accuracy of dye mediated EV labelling as an  
414 example of well-studied MSC-EV preparations. Upon analyzing labelled MSC-EV  
415 preparations by IFCM we demonstrated that none of the conventionally used dyes, BODIPY-  
416 TR-CER, Calcein AM, CFSE and PKH67 allowed accurate labelling of MSC-EVs. In contrast,  
417 the novel dye Exoria allowed the quantitative labelling of EVs within our MSC-EV  
418 preparations without interfering with their immunomodulatory properties as monitored in a  
419 multi-donor mixed lymphocyte reaction assay. Furthermore, upon removing unbound dye by  
420 ultrafiltration, EV up-taking cells were identified. Notably, CD81<sup>+</sup> EVs were stained more  
421 intensively with Exoria than CD63<sup>+</sup> EVs, indicating potential differences in membrane  
422 compositions of both EV subtypes which significantly influences their stainability. In this  
423 context it is worth mentioning that upon comparing the intensity of Exoria labelled HEK293T  
424 and THP-1 EVs in an ongoing study, almost all HEK293T cell EVs could be efficiently  
425 labelled, while most THP-1 EVs remain unstained (data not shown). Thus, even though  
426 Exoria appeared as a very useful dye for EVs within our MSC-EV preparations, it should not  
427 be considered a pan-EV labelling dye.

428 For now, the EV-field is just started exploring the heterogeneity within given EV preparations  
429 with pioneering work performed by bead capturing approaches mainly against tetraspanins  
430 or other EV surface proteins (Koliha et al., 2016a; Koliha et al., 2016b; Kowal et al., 2016).  
431 Another critical component of EVs that affects dye incorporation is the lipid composition of  
432 EV subtypes. Many studies have demonstrated that EV preparations from different cell  
433 sources have varied lipid compositions (Skotland et al., 2019; Skotland et al., 2017). These  
434 differences have been studied as potential biomarkers for cancers such as colorectal cancer

435 (Lydic et al., 2015), prostate cancer (Brzozowski et al., 2018) and Alzheimer disease (Su et  
436 al., 2020). Furthermore, many groups have utilized these differences to selectively capture  
437 EVs by utilizing different lipid binding molecules, i.e. chloral toxin B chain, Shiga toxin B  
438 subunit or Annexin V (Lai et al., 2016).

439 Whilst we were unable to identify the cause of the difference in EV subtype labelling, our  
440 study clearly demonstrates that experimenters need to critically (re)evaluate the  
441 appropriability of EV labelling dyes for their purposes. Using conventional technologies such  
442 as differential centrifugation protocols for the EV preparation or particle quantification  
443 devices, the specificity of the EV labelling dyes for the EVs of interest cannot be investigated  
444 (Simonsen, 2019). To this end, novel analysis devices are required, allowing EV analysis of  
445 dye stained and antibody labelled EVs. In addition to IFCM, other devices have entered the  
446 field allowing the colocalization of at least two different fluorescent labels on a single EV-  
447 sized object, including a novel generation of flow cytometers for nanoparticles such as the  
448 NanoFCM device (Tian et al., 2020) or nanoFACS (Morales-Kastresana et al., 2020),  
449 plasmon resonance devices with fluorescence detection units such as the NanoView device  
450 (Srinivasan et al., 2019) or novel direct stochastic optical reconstruction (dSTORM) devices  
451 such as the Nanoimager (Helmink et al., 2020) or the Nano Particle Tracking device in  
452 fluorescence mode. Indeed, elaborate analysis of EV labelling results performed on a NTA  
453 platform in the fluorescence mode has revealed discrepancies in the labelling of EVs with  
454 PKH. These results imply PKH uptake might not be connected to EVs (Dehghani et al., 2020;  
455 Lai et al., 2015). Upon characterizing of CFSE stained EV preparations of immature dendritic  
456 cells, CFSE was qualified as an appropriate labelling dye for these EVs (Morales-Kastresana  
457 et al., 2017b). Furthermore, EVs of different cell types differ in their esterase content, which  
458 effects the utility of CFSE labelling of generated EVs.

459 Overall, the results obtained in this and in other studies question the reliability of broadly  
460 used “EV labelling” dyes, challenging the interpretation of many EV studies which use dye-  
461 labelled EV preparations for the identification of potential EV target cells. For now, it is a  
462 common strategy in the field, to label EV preparations with “EV dyes” and perform uptake

463 experiments with the dye labelled EV preparations. In our opinion authors need to re-  
464 evaluate whether their EVs were indeed specifically labelled and whether the cells that took  
465 up labelled particles are indeed the target cells of the EVs. As such, EV uptake experiments  
466 remain extremely challenging. To the best of our understanding, the EVs within our MSC-EV  
467 preparations were accurately labelled, and we are confident that the Exoria labelled EVs  
468 were specifically taken up by the various immune cell types. However, it remains an open  
469 question, which of the labelled EV subtypes the cells took up most efficiently, be it CD9<sup>+</sup>,  
470 CD63<sup>+</sup> or CD81<sup>+</sup> EVs. We also consider that the different immune cell types may have  
471 preferences for different EV subtypes. Although our study fails to provide these answers, we  
472 hope that it helps to sensitize EV researchers around the globe for the challenges associated  
473 with the identification of EV target cells. Indeed, issues are further complicated by the fact  
474 that not necessarily all EV target cells take up EVs to process their signal. At least a  
475 proportion of EV mediated intercellular interactions might follow the *kiss and run* principle  
476 that EVs bind to receptor platforms on cells, activate these platforms and are shed off, similar  
477 to what has already been shown for synaptic vesicles (Chanaday et al., 2019; Wen et al.,  
478 2017).

## 479 **Acknowledgment**

480 We thank the Westdeutsche Spender Zentrale (WSZE) for providing bone marrow samples  
481 of healthy donors. We are grateful to the healthy blood donors whose cells were used in the  
482 mdMLR assay. This study was supported by funds of the European Union (ERA-NET  
483 EuroTransbio 11: EVTrust [031B0332B] and the European Union's Horizon 2020 research  
484 and innovation programme EVPRO under grant agreement No 814495 and AutoCRAT under  
485 grant agreement No 874671. The materials presented and views expressed here are the  
486 responsibility of the authors only. The EU Commission takes no responsibility for any use  
487 made of the information set out).

## 488 **Declaration of Interest Statement**

489 BG is a scientific advisory board member of Innovex Therapeutics SL and Mursla Ltd. and a  
490 founding director of Exosla Ltd. MS and PFJ are employees and shareholders of Exopharm  
491 Ltd. All other authors report no conflicts of interest.

## 492 **Contributions**

493 T.T., M.S., P.F.J. and B.G. conceived and planned the experiments; T.T. carried out the  
494 experiments with assistance provided by O.S. and A.A.-J.; T.T., M.S., P.F.J. and B.G.  
495 analyzed and interpreted experimental results; T.T. and B.G. wrote the manuscript. All  
496 authors provided critical feedback and approved the final version of the manuscript.

## 497 **References**

- 498 Banks, H.T., Choi, A., Huffman, T., Nardini, J., Poag, L., and Thompson, W.C. (2013).  
499 Quantifying CFSE Label Decay in Flow Cytometry Data. *Appl Math Lett* 26, 571-577.
- 500 Borger, V., Staubach, S., Dittrich, R., Stambouli, O., and Giebel, B. (2020). Scaled Isolation  
501 of Mesenchymal Stem/Stromal Cell-Derived Extracellular Vesicles. *Curr Protoc Stem Cell*  
502 *Biol* 55, e128.
- 503 Brzozowski, J.S., Jankowski, H., Bond, D.R., McCague, S.B., Munro, B.R., Predebon, M.J.,  
504 Scarlett, C.J., Skelding, K.A., and Weidenhofer, J. (2018). Lipidomic profiling of extracellular  
505 vesicles derived from prostate and prostate cancer cell lines. *Lipids in Health and Disease*  
506 17, 211.
- 507 Chanaday, N.L., Cousin, M.A., Milosevic, I., Watanabe, S., and Morgan, J.R. (2019). The  
508 Synaptic Vesicle Cycle Revisited: New Insights into the Modes and Mechanisms. *The*  
509 *Journal of Neuroscience* 39, 8209-8216.
- 510 Chuo, S.T.-Y., Chien, J.C.-Y., and Lai, C.P.-K. (2018). Imaging extracellular vesicles: current  
511 and emerging methods. *J Biomed Sci* 25, 91-91.
- 512 Dehghani, M., Gulvin, S.M., Flax, J., and Gaborski, T.R. (2020). Systematic Evaluation of  
513 PKH Labelling on Extracellular Vesicle Size by Nanoparticle Tracking Analysis. *Scientific*  
514 *Reports* 10, 9533.
- 515 Doeppner, T.R., Herz, J., Gorgens, A., Schlechter, J., Ludwig, A.K., Radtke, S., de  
516 Miroschedji, K., Horn, P.A., Giebel, B., and Hermann, D.M. (2015). Extracellular Vesicles  
517 Improve Post-Stroke Neuroregeneration and Prevent Postischemic Immunosuppression.  
518 *Stem Cells Transl Med* 4, 1131-1143.

519 Dragovic, R.A., Gardiner, C., Brooks, A.S., Tannetta, D.S., Ferguson, D.J., Hole, P., Carr, B.,  
520 Redman, C.W., Harris, A.L., Dobson, P.J., *et al.* (2011). Sizing and phenotyping of cellular  
521 vesicles using Nanoparticle Tracking Analysis. *Nanomedicine* 7, 780-788.

522 Drommelschmidt, K., Serdar, M., Bendix, I., Herz, J., Bertling, F., Prager, S., Keller, M.,  
523 Ludwig, A.K., Duhan, V., Radtke, S., *et al.* (2017). Mesenchymal stem cell-derived  
524 extracellular vesicles ameliorate inflammation-induced preterm brain injury. *Brain Behav*  
525 *Immun* 60, 220-232.

526 Droste, M., Tertel, T., Jeruschke, S., Dittrich, R., Kontopoulou, E., Walkenfort, B., Börger, V.,  
527 Hoyer, P.F., Büscher, A.K., Thakur, B.K., *et al.* (2021). Single extracellular vesicle analysis  
528 performed by imaging flow cytometry in contrast to NTA rigorously assesses the accuracy of  
529 urinary extracellular vesicle preparation techniques. *bioRxiv*, 2021.2004.2001.437817.

530 Fais, S., O'Driscoll, L., Borrás, F.E., Buzas, E., Camussi, G., Cappello, F., Carvalho, J.,  
531 Cordeiro da Silva, A., Del Portillo, H., El Andaloussi, S., *et al.* (2016). Evidence-Based  
532 Clinical Use of Nanoscale Extracellular Vesicles in Nanomedicine. *ACS Nano* 10, 3886-3899.

533 Giebel, B., and Helmbrecht, C. (2017). Methods to Analyze EVs. *Methods in molecular*  
534 *biology (Clifton, NJ)* 1545, 1-20.

535 Görgens, A., Bremer, M., Ferrer-Tur, R., Murke, F., Tertel, T., Horn, P.A., Thalmann, S.,  
536 Welsh, J.A., Probst, C., Guerin, C., *et al.* (2019). Optimisation of imaging flow cytometry for  
537 the analysis of single extracellular vesicles by using fluorescence-tagged vesicles as  
538 biological reference material. *J Extracell Vesicles* 8, 1587567.

539 Gray, W.D., Mitchell, A.J., and Searles, C.D. (2015). An accurate, precise method for general  
540 labelling of extracellular vesicles. *MethodsX* 2, 360-367.

541 Gussenhoven, R., Klein, L., Ophelders, D., Habets, D.H.J., Giebel, B., Kramer, B.W.,  
542 Schurgers, L.J., Reutelingsperger, C.P.M., and Wolfs, T. (2019). Annexin A1 as  
543 Neuroprotective Determinant for Blood-Brain Barrier Integrity in Neonatal Hypoxic-Ischemic  
544 Encephalopathy. *J Clin Med* 8.

545 Helminck, B.A., Reddy, S.M., Gao, J., Zhang, S., Basar, R., Thakur, R., Yizhak, K., Sade-  
546 Feldman, M., Blando, J., Han, G., *et al.* (2020). B cells and tertiary lymphoid structures  
547 promote immunotherapy response. *Nature* 577, 549-555.

548 Kaminski, N., Koster, C., Mouloud, Y., Borger, V., Felderhoff-Muser, U., Bendix, I., Giebel,  
549 B., and Herz, J. (2020). Mesenchymal Stromal Cell-Derived Extracellular Vesicles Reduce  
550 Neuroinflammation, Promote Neural Cell Proliferation and Improve Oligodendrocyte  
551 Maturation in Neonatal Hypoxic-Ischemic Brain Injury. *Front Cell Neurosci* 14, 601176.

552 Karimi, N., Cvjetkovic, A., Jang, S.C., Crescitelli, R., Hosseinpour Feizi, M.A., Nieuwland, R.,  
553 Lotvall, J., and Lasser, C. (2018). Detailed analysis of the plasma extracellular vesicle  
554 proteome after separation from lipoproteins. *Cell Mol Life Sci* 75, 2873-2886.

555 Koliha, N., Heider, U., Ozimkowski, T., Wiemann, M., Bosio, A., and Wild, S. (2016a).  
556 Melanoma Affects the Composition of Blood Cell-Derived Extracellular Vesicles. *Front*  
557 *Immunol* 7, 282.

558 Koliha, N., Wiencek, Y., Heider, U., Jungst, C., Kladt, N., Krauthauser, S., Johnston, I.C.,  
559 Bosio, A., Schauss, A., and Wild, S. (2016b). A novel multiplex bead-based platform  
560 highlights the diversity of extracellular vesicles. *J Extracell Vesicles* 5, 29975.

561 König, L., Kasimir-Bauer, S., Bittner, A.-K., Hoffmann, O., Wagner, B., Santos Manvailer,  
562 L.F., Kimmig, R., Horn, P.A., and Rebmann, V. (2018). Elevated levels of extracellular  
563 vesicles are associated with therapy failure and disease progression in breast cancer  
564 patients undergoing neoadjuvant chemotherapy. *OncolImmunology* 7, e1376153.

565 Kordelas, L., Rebmann, V., Ludwig, A.K., Radtke, S., Ruesing, J., Doeppner, T.R., Epple, M.,  
566 Horn, P.A., Beelen, D.W., and Giebel, B. (2014). MSC-derived exosomes: a novel tool to  
567 treat therapy-refractory graft-versus-host disease. *Leukemia* 28, 970-973.

568 Kowal, J., Arras, G., Colombo, M., Jouve, M., Morath, J.P., Primdal-Bengtson, B., Dingli, F.,  
569 Loew, D., Tkach, M., and Thery, C. (2016). Proteomic comparison defines novel markers to  
570 characterize heterogeneous populations of extracellular vesicle subtypes. *Proc Natl Acad Sci*  
571 *U S A* 113, E968-977.



572 Lai, C.P., Kim, E.Y., Badr, C.E., Weissleder, R., Mempel, T.R., Tannous, B.A., and  
573 Breakefield, X.O. (2015). Visualization and tracking of tumour extracellular vesicle delivery  
574 and RNA translation using multiplexed reporters. *Nat Commun* 6, 7029.

575 Lai, R.C., Tan, S.S., Yeo, R.W., Choo, A.B., Reiner, A.T., Su, Y., Shen, Y., Fu, Z., Alexander,  
576 L., Sze, S.K., *et al.* (2016). MSC secretes at least 3 EV types each with a unique permutation  
577 of membrane lipid, protein and RNA. *J Extracell Vesicles* 5, 29828.

578 Laulagnier, K., Vincent-Schneider, H., Hamdi, S., Subra, C., Lankar, D., and Record, M.  
579 (2005). Characterization of exosome subpopulations from RBL-2H3 cells using fluorescent  
580 lipids. *Blood cells, molecules & diseases* 35, 116-121.

581 Ludwig, A.K., De Miroschedji, K., Doepfner, T.R., Borger, V., Ruesing, J., Rebmann, V.,  
582 Durst, S., Jansen, S., Bremer, M., Behrmann, E., *et al.* (2018). Precipitation with  
583 polyethylene glycol followed by washing and pelleting by ultracentrifugation enriches  
584 extracellular vesicles from tissue culture supernatants in small and large scales. *J Extracell*  
585 *Vesicles* 7, 1528109.

586 Lydic, T.A., Townsend, S., Adda, C.G., Collins, C., Mathivanan, S., and Reid, G.E. (2015).  
587 Rapid and comprehensive 'shotgun' lipidome profiling of colorectal cancer cell derived  
588 exosomes. *Methods* 87, 83-95.

589 Madel, R.J., Börger, V., Dittrich, R., Bremer, M., Tertel, T., Phuong, N.N.T., Baba, H.A.,  
590 Kordelas, L., Buer, J., Horn, P.A., *et al.* (2020). Independent human mesenchymal stromal  
591 cell-derived extracellular vesicle preparations differentially affect symptoms in an advanced  
592 murine Graft-versus-Host-Disease model. *bioRxiv*, 2020.2012.2021.423658.

593 Morales-Kastresana, A., Telford, B., Musich, T.A., McKinnon, K., Clayborne, C., Braig, Z.,  
594 Rosner, A., Demberg, T., Watson, D.C., Karpova, T.S., *et al.* (2017a). Labelling Extracellular  
595 Vesicles for Nanoscale Flow Cytometry. *Sci Rep* 7, 1878.

596 Morales-Kastresana, A., Telford, B., Musich, T.A., McKinnon, K., Clayborne, C., Braig, Z.,  
597 Rosner, A., Demberg, T., Watson, D.C., Karpova, T.S., *et al.* (2017b). Labelling Extracellular  
598 Vesicles for Nanoscale Flow Cytometry. *Scientific Reports* 7, 1878.

599 Morales-Kastresana, A., Welsh, J.A., and Jones, J.C. (2020). Detection and Sorting of  
600 Extracellular Vesicles and Viruses Using nanoFACS. *Curr Protoc Cytom* 95, e81.

601 Nazarenko, I., Rupp, A.K., and Altevogt, P. (2013). Exosomes as a potential tool for a  
602 specific delivery of functional molecules. *Methods in molecular biology (Clifton, NJ)* 1049,  
603 495-511.

604 Ophelders, D.R., Wolfs, T.G., Jellema, R.K., Zwanenburg, A., Andriessen, P., Delhaas, T.,  
605 Ludwig, A.K., Radtke, S., Peters, V., Janssen, L., *et al.* (2016). Mesenchymal Stromal Cell-  
606 Derived Extracellular Vesicles Protect the Fetal Brain After Hypoxia-Ischemia. *Stem Cells*  
607 *Transl Med* 5, 754-763.

608 Pospichalova, V., Svoboda, J., Dave, Z., Kotrbova, A., Kaiser, K., Klemova, D., Ilkovic, L.,  
609 Hampl, A., Crha, I., Jandakova, E., *et al.* (2015). Simplified protocol for flow cytometry  
610 analysis of fluorescently labelled exosomes and microvesicles using dedicated flow  
611 cytometer. *J Extracell Vesicles* 4, 25530.

612 Pužar Dominkuš, P., Stenovec, M., Sitar, S., Lasič, E., Zorec, R., Plemenitaš, A., Žagar, E.,  
613 Kreft, M., and Lenassi, M. (2018). PKH26 labelling of extracellular vesicles: Characterization  
614 and cellular internalization of contaminating PKH26 nanoparticles. *Biochimica et biophysica*  
615 *acta Biomembranes* 1860, 1350-1361.

616 Raposo, G., and Stoorvogel, W. (2013). Extracellular vesicles: exosomes, microvesicles, and  
617 friends. *J Cell Biol* 200, 373-383.

618 Simonsen, J.B. (2019). Pitfalls associated with lipophilic fluorophore staining of extracellular  
619 vesicles for uptake studies. *J Extracell Vesicles* 8, 1582237.

620 Skotland, T., Hessvik, N.P., Sandvig, K., and Llorente, A. (2019). Exosomal lipid composition  
621 and the role of ether lipids and phosphoinositides in exosome biology. *J Lipid Res* 60, 9-18.

622 Skotland, T., Sandvig, K., and Llorente, A. (2017). Lipids in exosomes: Current knowledge  
623 and the way forward. *Prog Lipid Res* 66, 30-41.

624 Sokolova, V., Ludwig, A.-K., Hornung, S., Rotan, O., Horn, P.A., Epple, M., and Giebel, B.  
625 (2011). Characterisation of exosomes derived from human cells by nanoparticle tracking

626 analysis and scanning electron microscopy. *Colloids and Surfaces B: Biointerfaces* 87, 146-  
627 150.

628 Srinivasan, S., Yeri, A., Cheah, P.S., Chung, A., Danielson, K., De Hoff, P., Filant, J.,  
629 Laurent, C.D., Laurent, L.D., Magee, R., *et al.* (2019). Small RNA Sequencing across  
630 Diverse Biofluids Identifies Optimal Methods for exRNA Isolation. *Cell* 177, 446-462.e416.

631 Su, H., Rustam, Y.H., Masters, C.L., Makalic, E., McLean, C., Hill, A.F., Barnham, K.J., Reid,  
632 G.E., and Vella, L.J. (2020). Characterization of Brain-Derived Extracellular Vesicle Lipids in  
633 Alzheimer's Disease. *bioRxiv*, 2020.2008.2020.260356.

634 Tertel, T., Bremer, M., Maire, C., Lamszus, K., Peine, S., Jawad, R., Andaloussi, S.E.L.,  
635 Giebel, B., Ricklefs, F.L., and Gorgens, A. (2020a). High-Resolution Imaging Flow Cytometry  
636 Reveals Impact of Incubation Temperature on Labelling of Extracellular Vesicles with  
637 Antibodies. *Cytometry A* 97, 602-609.

638 Tertel, T., Gorgens, A., and Giebel, B. (2020b). Chapter Four - Analysis of individual  
639 extracellular vesicles by imaging flow cytometry. In *Methods in Enzymology*, S. Spada, and  
640 L. Galluzzi, eds. (Academic Press), pp. 55-78.

641 Thery, C., Witwer, K.W., Aikawa, E., Alcaraz, M.J., Anderson, J.D., Andriantsitohaina, R.,  
642 Antoniou, A., Arab, T., Archer, F., Atkin-Smith, G.K., *et al.* (2018). Minimal information for  
643 studies of extracellular vesicles 2018 (MISEV2018): a position statement of the International  
644 Society for Extracellular Vesicles and update of the MISEV2014 guidelines. *J Extracell*  
645 *Vesicles* 7, 1535750.

646 Tian, Y., Gong, M., Hu, Y., Liu, H., Zhang, W., Zhang, M., Hu, X., Aubert, D., Zhu, S., Wu, L.,  
647 *et al.* (2020). Quality and efficiency assessment of six extracellular vesicle isolation methods  
648 by nano-flow cytometry. *J Extracell Vesicles* 9, 1697028.

649 Vacchi, E., Burrello, J., Di Silvestre, D., Burrello, A., Bolis, S., Mauri, P., Vassalli, G., Cereda,  
650 C.W., Farina, C., Barile, L., *et al.* (2020). Immune profiling of plasma-derived extracellular  
651 vesicles identifies Parkinson disease. *Neurology - Neuroimmunology Neuroinflammation* 7,  
652 e866.

653 van der Pol, E., Coumans, F.A.W., Grootemaat, A.E., Gardiner, C., Sargent, I.L., Harrison,  
654 P., Sturk, A., van Leeuwen, T.G., and Nieuwland, R. (2014). Particle size distribution of  
655 exosomes and microvesicles determined by transmission electron microscopy, flow  
656 cytometry, nanoparticle tracking analysis, and resistive pulse sensing. *Journal of Thrombosis*  
657 *and Haemostasis* 12, 1182-1192.

658 Vergauwen, G., Dhondt, B., Van Deun, J., De Smedt, E., Berx, G., Timmerman, E., Gevaert,  
659 K., Miinalainen, I., Cocquyt, V., Braems, G., *et al.* (2017). Confounding factors of  
660 ultrafiltration and protein analysis in extracellular vesicle research. *Sci Rep* 7, 2704.

661 Wang, C., Borger, V., Sardari, M., Murke, F., Skuljec, J., Pul, R., Hagemann, N., Dzyubenko,  
662 E., Dittrich, R., Gregorius, J., *et al.* (2020). Mesenchymal Stromal Cell-Derived Small  
663 Extracellular Vesicles Induce Ischemic Neuroprotection by Modulating Leukocytes and  
664 Specifically Neutrophils. *Stroke* 51, 1825-1834.

665 Welsh, J.A., Van Der Pol, E., Arkesteijn, G.J.A., Bremer, M., Brisson, A., Coumans, F.,  
666 Dignat-George, F., Duggan, E., Ghiran, I., Giebel, B., *et al.* (2020). MIFlowCyt-EV: a  
667 framework for standardized reporting of extracellular vesicle flow cytometry experiments.  
668 *Journal of Extracellular Vesicles* 9, 1713526.

669 Wen, X., Saltzgaber, G.W., and Thoreson, W.B. (2017). Kiss-and-Run Is a Significant  
670 Contributor to Synaptic Exocytosis and Endocytosis in Photoreceptors. *Frontiers in cellular*  
671 *neuroscience* 11, 286-286.

672 Wiklander, O.P.B., Bostancioglu, R.B., Welsh, J.A., Zickler, A.M., Murke, F., Corso, G.,  
673 Felldin, U., Hagey, D.W., Evertsson, B., Liang, X.M., *et al.* (2018). Systematic Methodological  
674 Evaluation of a Multiplex Bead-Based Flow Cytometry Assay for Detection of Extracellular  
675 Vesicle Surface Signatures. *Front Immunol* 9, 1326.

676 Yanez-Mo, M., Siljander, P.R., Andreu, Z., Zavec, A.B., Borrás, F.E., Buzas, E.I., Buzas, K.,  
677 Casal, E., Cappello, F., Carvalho, J., *et al.* (2015). Biological properties of extracellular  
678 vesicles and their physiological functions. *J Extracell Vesicles* 4, 27066.

679